









Reversible dehydrogenation and rehydrogenation of cyclohexane and methylcyclohexane by single-site platinum catalyst

Luning Chen^{1,2,3,8}, Pragya Verma^{1,8}, Kaipeng Hou^{4,8}, Zhiyuan Qi³, Shuchen Zhang³, Yi-Sheng Liu ⁵, Jinghua Guo ⁵, Vitalie Stavila ⁶, Mark D. Allendorf ⁶, Lansun Zheng², Miquel Salmeron ^{3,7}, David Prendergast ¹✉, Gabor A. Somorjai ^{3,4}✉ & Ji Su ^{1,3}✉

Developing highly efficient and reversible hydrogenation-dehydrogenation catalysts shows great promise for hydrogen storage technologies with highly desirable economic and ecological benefits. Herein, we show that reaction sites consisting of single Pt atoms and neighboring oxygen vacancies (V_O) can be prepared on CeO_2 (Pt_1/CeO_2) with unique catalytic properties for the reversible dehydrogenation and rehydrogenation of large molecules such as cyclohexane and methylcyclohexane. Specifically, we find that the dehydrogenation rate of cyclohexane and methylcyclohexane on such sites can reach values above $32,000 \text{ mol}_{H_2} \text{ mol}_{Pt}^{-1} \text{ h}^{-1}$, which is 309 times higher than that of conventional supported Pt nanoparticles. Combining of DRIFTS, AP-XPS, EXAFS, and DFT calculations, we show that the Pt_1/CeO_2 catalyst exhibits a super-synergistic effect between the catalytic Pt atom and its support, involving redox coupling between Pt and Ce ions, enabling adsorption, activation and reaction of large molecules with sufficient versatility to drive abstraction/addition of hydrogen without requiring multiple reaction sites.

¹The Molecular Foundry, Lawrence Berkeley National Laboratory, Berkeley, CA 94720, USA. ²State Key Laboratory of Physical Chemistry of Solid Surfaces, Collaborative Innovation Center of Chemistry for Energy Materials, and Department of Chemistry, College of Chemistry and Chemical Engineering, Xiamen University, 361005 Xiamen, China. ³Chemical Sciences Division, Lawrence Berkeley National Laboratory, Berkeley, CA 94720, USA. ⁴Department of Chemistry, University of California-Berkeley, Berkeley, CA 94720, USA. ⁵Advanced Light Source, Lawrence Berkeley National Laboratory, Berkeley, CA 94720, USA. ⁶Sandia National Laboratories, Livermore, CA 94551, USA. ⁷Materials Science and Engineering Department, University of California-Berkeley, Berkeley, CA 94720, USA. ⁸These authors contributed equally: Luning Chen, Pragya Verma, Kaipeng Hou. ✉email: dgprendergast@lbl.gov; somorjai@berkeley.edu; jisu@lbl.gov

Metal particles on various supports play a central role in energy conversion reactions and chemical transformations by heterogeneous catalysis. Ideally, the support immobilizes the particles reducing their mobility to prevent sintering, and favoring chemical stabilization¹. Active supports, consisting of reducible oxides participate in the catalytic reaction through metal-support interactions involving charge transfer between metal particles and support, harboring multi-functional active centers, and mediating spillover of reactants and products^{2–4}. Recently, the creation of single-site catalysts^{5–7}, where single metal atoms are anchored on support by bonding to ligands such as N or O, has opened up a new research frontier in the catalysis field^{8–10}. The isolated metal sites provide a bridge between heterogeneous and homogeneous catalysis¹¹. Reduction of the size of metal nanoparticles down to a single atom achieves the maximum efficiency of utilization of expensive noble metals, with gains in activity, stability, and selectivity^{12–14}. However, the lack of an ensemble of other active sites adjacent to the single noble metal atom may prevent surface reactions that involve large molecules^{15,16}. Recent studies demonstrated that “ensemble effects” between the single metal atom and neighboring oxygen vacancies can favor oxygen transfer and adsorption of reactants, enabling catalysis reactions of the functional groups on large molecules with higher efficiency^{17–19}. The beneficial effect of oxygen vacancy sites next to the noble metal^{12,14} motivated us to further explore its possibilities with the goal to discover new reactions and to accelerate the development of next-generation single-site catalysts.

Hydrogen is an ideal fuel for clean energy, replacing traditional hydrocarbon feedstocks. It is also used in polymer electrolyte membrane fuel cells (PEMFCs) because of its high mass-energy density of 141.6 MJ/kg, three times higher than that of gasoline, while producing water as the only by-product^{20–22}. The challenges of these applications are associated with the difficulties of efficient hydrogen storage, which today are mostly based on compression and liquefaction technologies, introducing safety concerns and low storage density, as well as transportation, boil-off losses, and other high-cost problems²³. Liquid organic hydrogen carriers (LOHCs) represent an attractive alternative to store hydrogen in chemical bonds and can address a number of limitations of present technologies²⁴. Reversible LOHC systems are always composed of pairs of hydrogen-poor and hydrogen-rich organic compounds that store hydrogen by hydrogenation and dehydrogenation²⁵, which has a high potential for mobile applications²⁶. Cycloalkanes and aromatics with one or more six-membered rings are promising reversible LOHC systems. These stable compounds have high storage capacities (between 6 and 7 wt.% H₂) and can be dehydrogenated/rehydrogenated under relatively mild conditions^{27,28}. Supported Pt nanoparticle catalysts are industrially mature and superior heterogeneous catalysts used in hydrocarbon refineries^{29,30}. Based on a sulfated Pt nanoparticle catalyst (S-Pt/Al₂O₃), Chiyoda Corporation developed a LOHC system with dehydrogenation/rehydrogenation of methylcyclohexane (MCH)/toluene and demonstrated its feasibility and advantage for hydrogen storage and transportation³¹. Nevertheless, the high cost and low natural abundance of Pt limited its further application. Downsizing of Pt from nanoparticle to single atoms is an effective method to maximize the Pt atom efficiency and reduce this component of the capital investment.

In this work, we show the successful fabrication and demonstration of isolated single Pt atoms on CeO₂ (Pt₁/CeO₂) that is highly efficient and reversible for dehydrogenation/rehydrogenation of large cyclic hydrocarbons. As we will show, compared with traditional Pt nanoparticle catalysts (several nm in size on CeO₂), the single Pt atom catalyst displays significantly

higher catalytic performance for both dehydrogenation and rehydrogenation reactions. In particular, the turnover frequency (TOF) of cyclohexane and methylcyclohexane on such single Pt sites could reach >32,000 mol H₂ per mol Pt per hour (5.5 g_{H₂} g_{Pt}⁻¹ min⁻¹), which is 309 times that of commercial Pt/Al₂O₃ (5 wt.%) catalyst. Key to this high performance is the discovery that oxygen vacancies next to the Pt atom site facilitate adsorption of these large cyclic molecules and stepwise dehydrogenation reactions driven by a super-synergistic effect involving redox coupling between Pt and Ce atoms.

Results and discussion

Preparation and characterization of isolated single Pt sites on CeO₂ (Pt₁/CeO₂). The Pt₁/CeO₂ catalyst was fabricated by a modified ascorbic acid (AA)-assisted reduction method, described in detail in the methods section³². Porous CeO₂ nanorods were synthesized and employed as supports to isolate Pt single sites due to their high specific area. Inductively Coupled Plasma Optical Emission Spectroscopy (ICP-OES) measurements revealed that the final content of Pt was 0.15 wt.%.

After deposition of Pt on CeO₂, no peaks from Pt were observed in the powder X-ray diffraction (XRD) pattern, due to the low Pt content and small size of the particles that may be present (Supplementary Fig. 1). Moreover, no difference was observed, relative to the original CeO₂ nanorods, in bright-field transmission electron microscopy (TEM) images, indicating that the number of such Pt nanoparticles or clusters is below the detection limit (Supplementary Fig. 1). However, elemental mapping of Pt₁/CeO₂ catalyst by HAADF-STEM, shows that Pt is present and uniformly distributed on the CeO₂ nanorods (Fig. 1a). More importantly, Cs-corrected HAADF-STEM images reveal the presence of isolated Pt single sites (white circles), which are brighter compared to surrounding Ce due to their larger atomic number, and dispersed throughout the porous CeO₂ support, as shown in Fig. 1b^{5,32}. Important additional information was obtained from X-ray absorption spectroscopy at the Pt L₃ edge, in experiments with Pt foils, PtO₂ as a reference, and with the Pt₁/CeO₂ catalyst. The near-edge fine structure (XANES) provides insights into the valence state of Pt (Fig. 1c), while the extended X-ray adsorption fine structure part (EXAFS) provides information on the local bonding geometry³³. The EXAFS data from the Pt₁/CeO₂ catalyst show only one peak from Pt-O bonds around 1.5 Å, but no Pt-Pt bonds could be detected, as shown by comparison with the reference bulk PtO₂ and Pt foil (Fig. 1d). Details of the EXAFS fitting results are listed in Supplementary Table 1. The combined evidence from Cs-corrected HAADF-STEM and EXAFS strongly support the conclusion that the Pt in the Pt₁/CeO₂ catalyst is largely present as isolated single atoms on CeO₂ while no metallic particles or clusters are present in detectable amounts. In more detail, compared with the PtO₂ reference, although there is not an obvious white line shift of Pt₁/CeO₂ due to the low Pt concentration on the surface and detector limitation, the lower energy shoulder (Fig. 1) indicates that the Pt oxidation state in Pt₁/CeO₂ is lower than +4³⁴, in agreement with the ambient-pressure X-ray photoelectron spectroscopy (AP-XPS) results. These low oxidation state Pt species are critical to our proposed mechanism below, especially in the initial stage of the reaction.

Dehydrogenation of cyclohexane. As a reversible LOHC system, cyclohexane/benzene is ideal for the storage and transportation of hydrogen. Here we used the as-prepared Pt₁/CeO₂ single-site catalyst for the catalytic cyclohexane dehydrogenation reaction (Supplementary Fig. 2). The catalyst showed excellent activity compared to that of Pt nanoparticles on CeO₂ (2.5 nm Pt/CeO₂)

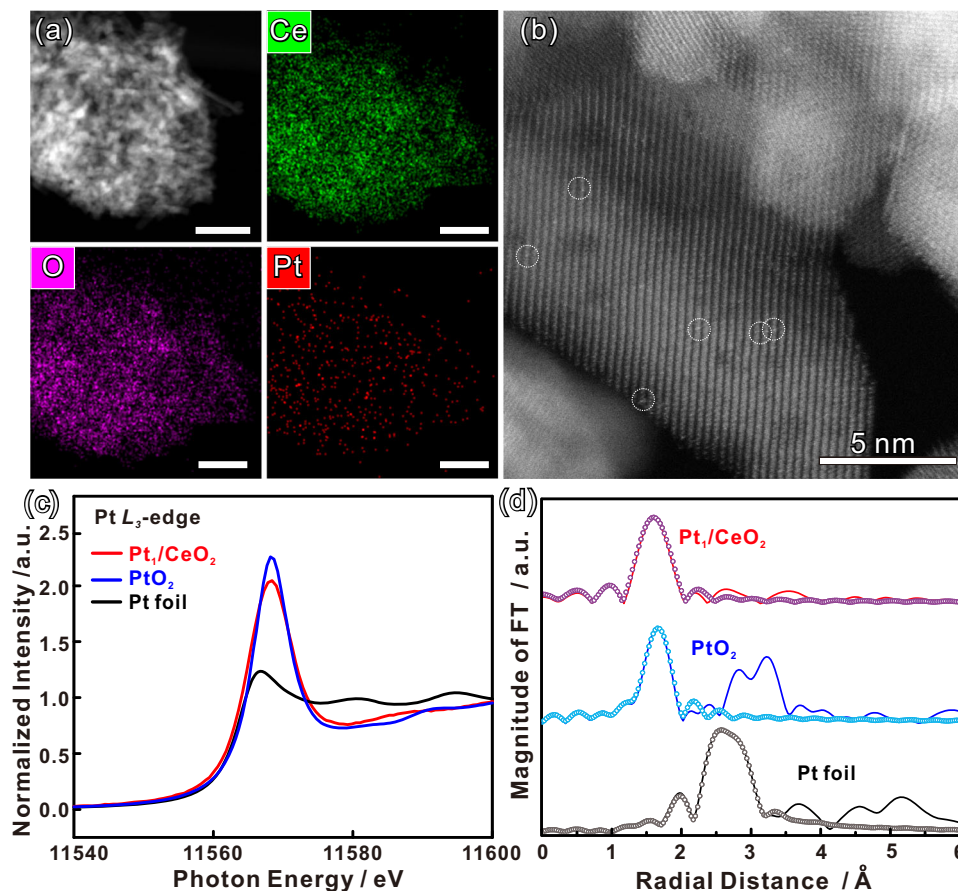


Fig. 1 Morphology and structural characterization of Pt₁/CeO₂ catalysts. **a** High-angle annular dark-field scanning transmission electron microscopy (HAADF-STEM) images and corresponding elemental map images of the Pt₁/CeO₂ catalyst (scale bars = 50 nm). **b** Cs-corrected HAADF-STEM images of the Pt₁/CeO₂ catalyst. The brighter dots (circled) are from Pt single sites. **c** Normalized Pt L₃-edge XANES spectra, and **d** *k*³-weighted Fourier transform EXAFS spectra (L₃-edge) of Pt in Pt₁/CeO₂, PtO₂, and bulk Pt foil at the Pt L₃-edge. The circles are fit to the data.

and 7.0 nm Pt/CeO₂), which were synthesized according to previous work (Supplementary Fig. 3)²⁶. At temperatures below 100 °C all the catalysts were inactive. When the temperature increased to 100 °C hydrogen was generated at measurable rates from the dehydrogenation of cyclohexane on the Pt₁/CeO₂ catalyst. With further increase in temperature, the TOF of hydrogen generation by cyclohexane dehydrogenation increased, reaching 32,477 mol_{H₂} mol_{Pt}⁻¹ h⁻¹ (5.5 g_{H₂} g_{Pt}⁻¹ min⁻¹) at 350 °C (Fig. 2a), which is 309-fold higher than that of commercial Pt particles on aluminum oxide catalysts with 5% loading (Fig. 3). In contrast, no catalytic activity was detected with Pt nanoparticles of 2.5 nm and 7.0 nm size on CeO₂ until the temperature increased to 400 °C (Fig. 3, Supplementary Table 2). To further assess the catalytic performance of Pt₁/CeO₂, we measured the TOF of hydrogen generation and conversion from cyclohexane at 350 °C at different cyclohexane feed rates (Fig. 2b). At low feed rates (0.01 mL/min), the conversion of cyclohexane reached 100%, with a TOF around 10,900 mol_{H₂} mol_{Pt}⁻¹ h⁻¹ (1.9 g_{H₂} g_{Pt}⁻¹ min⁻¹). Alternatively, a higher TOF around 35,400 mol_{H₂} mol_{Pt}⁻¹ h⁻¹ (6.0 g_{H₂} g_{Pt}⁻¹ min⁻¹) was achieved at feed rates of 0.1 mL/min. As shown in the literature, the equilibrium constant (*K*_{eq}) of the dehydrogenation of cycloalkanes under an ambient pressure only depends on the reaction temperature³⁵. And the equilibrium conversion for the dehydrogenation of cyclohexane and methylcyclohexane could reach 99% above 593 K. In our study, the highest conversion at 350 °C is around 30% (Fig. 2a), which is much lower than the equilibrium conversion. Therefore,

the reaction TOF could reach values as high as 32,000–35,200 mol H₂ per mol Pt per hour. These results illustrate the excellent catalytic activity of Pt₁/CeO₂ catalyst, and its potential for process scale-up. Moreover, the single-site Pt₁/CeO₂ catalyst exhibited remarkably high selectivity towards benzene production in the cyclohexane dehydrogenation reaction. At temperatures of 150 °C and 200 °C, the major dehydrogenated product (more than 80%) was benzene with <20% of cyclohexene detected. When the temperature was above 250 °C, essentially only dehydrogenation product is benzene (Fig. 2c).

For practical applications, stability and recyclability are important parameters when evaluating long-term catalyst performance. After 72 h at 350 °C with 3 mL/h cyclohexane feeding rate, the Pt₁/CeO₂ catalyst still maintains more than 90% of its original activity (Fig. 2d), the small decrease of activity results from the loss of some Pt species on CeO₂²⁶. The recyclability of Pt₁/CeO₂ catalyst was assessed by cyclic cyclohexane dehydrogenation experiments (Supplementary Fig. 4). The results indicate that there is no obvious activity decay during four cycles of cyclohexane dehydrogenation under different temperatures. EXAFS was also employed to confirm that the structure of Pt₁/CeO₂ remained stable after long reaction times and after repeated cycles of catalytic reaction. No apparent difference was found between used and freshly prepared Pt₁/CeO₂ catalysts, indicating that during reaction the fine structure of the Pt₁/CeO₂ remains unchanged (Supplementary Fig. 5). We attribute the high stability to the embedded nature of the Pt into the CeO₂ surface layer, which is produced by

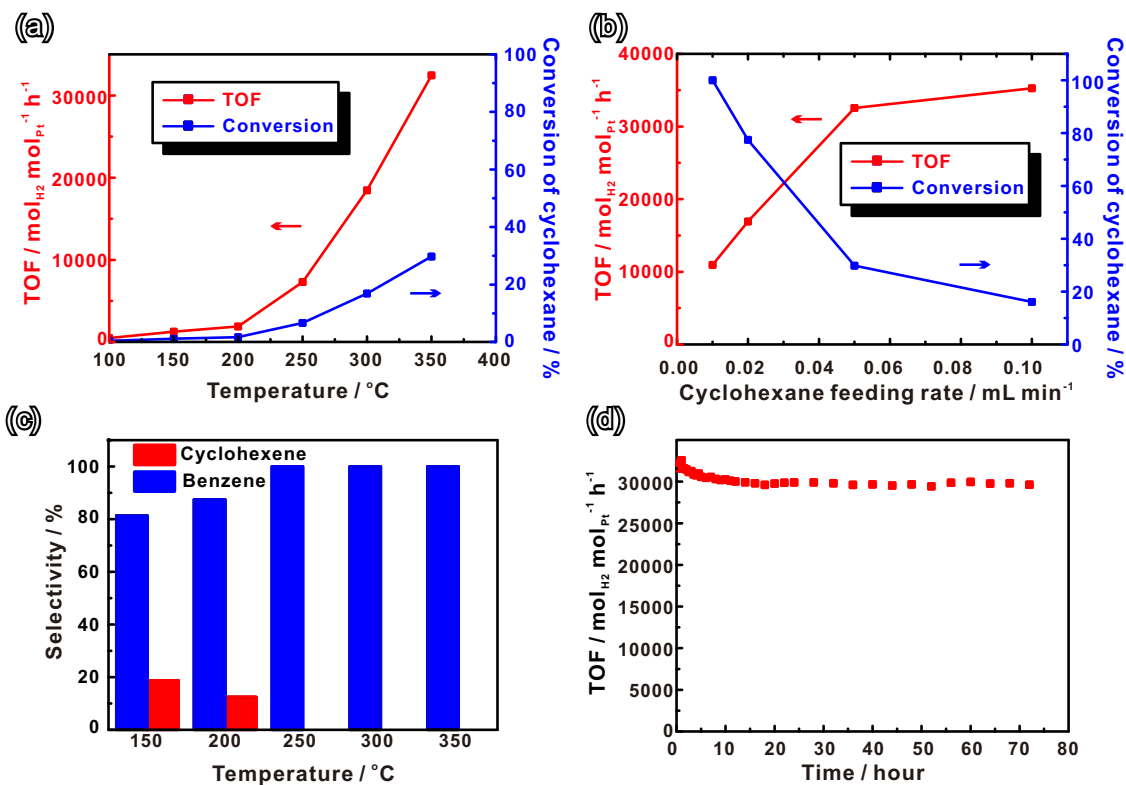


Fig. 2 Catalytic cyclohexane dehydrogenation performance of Pt₁/CeO₂. **a** Turnover frequency (TOF) of hydrogen production per mol Pt of Pt₁/CeO₂ and conversion of cyclohexane at different temperatures. Reaction conditions: **b** turnover frequency (TOF) of hydrogen production per mol Pt of Pt₁/CeO₂ and conversion of cyclohexane at 350 °C for different cyclohexane feeding rates. **c** Selectivity of cyclohexane dehydrogenation at different temperatures. **d** Turnover frequency (TOF) of hydrogen production per mol Pt of Pt₁/CeO₂ at 350 °C during 72 h of reaction.

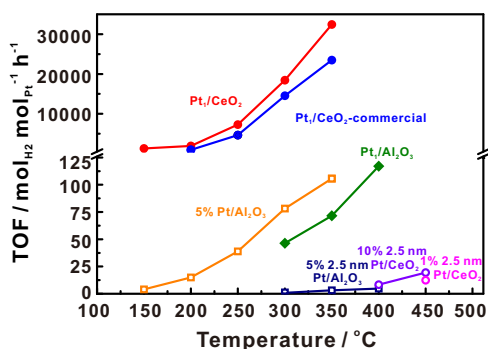


Fig. 3 Comparison Pt₁/CeO₂ catalytic performance with other catalysts.

Turnover frequency (TOF) of hydrogen production per Pt site of different catalysts as a function of temperature. The circle symbols correspond to supports with cyclohexane adsorption ability while square symbols correspond to supports with no cyclohexane adsorption ability. Solid symbols denote single Pt site catalysts while hollow symbols denote Pt nanoparticle catalysts.

depositing it on a high surface area of CeO₂ at relatively low Pt loading amounts^{36,37}. In addition, the abundant Ce³⁺ species further increase the stability of Pt₁/CeO₂ catalysts³⁸. However, increasing the temperature to 400 °C resulted in a decrease in reaction activity as a result of some Pt aggregation and carbon deposition, as revealed by EXAFS (Supplementary Figs. 5, 6).

Cyclohexane dehydrogenation on different catalysts. It has been reported that single-site catalysts have limitations for reactions

involving large molecules due to the lack of surrounding ensemble sites to accommodate the molecule and its products. However, our results show that the single-site Pt₁/CeO₂ is 309 times more active than Pt particles supported on CeO₂ or Al₂O₃, which ranks the highest among the reported catalysts (Supplementary Fig. 7)³⁹. To understand this effect and the reaction mechanism, a comparison of the performance of Pt and its different ensemble size effects in different supports is needed. We tested the dehydrogenation reaction of cyclohexane on a series of catalysts such as different Pt nanoparticles of different sizes on CeO₂, single-site Pt on Al₂O₃, and commercial Pt catalysts (5% Pt/Al₂O₃) (Fig. 3, Supplementary Fig. 8, and Supplementary Table 2). We found that on different Pt nanoparticles sizes (2.5 nm and 7 nm) loaded on CeO₂, different pretreatments, and different Pt content, there was no hydrogen detected until the temperature was higher than 400 °C. Moreover, for single-site Pt on Al₂O₃ (Pt₁/Al₂O₃), which was synthesized following literature reports⁴⁰, we found that although the Pt is also in single-atom form, its catalytic activity is much lower than that of Pt₁/CeO₂, indicating the aforementioned super-synergistic role played by the support in case of Pt₁/CeO₂.

To further elucidate the role of the support in the dehydrogenation reaction we used in situ DRIFTS to study cyclohexane adsorption and desorption⁴¹. The results showed that the as-prepared Pt₁/CeO₂ support exhibited much stronger adsorption of cyclohexane as compared to that of Pt₁/Al₂O₃ (Supplementary Fig. 9). Due to the strong interaction between CeO₂ and cyclohexane, after stopping the flow of cyclohexane and purging with pure N₂ for 40 min, there are still two peaks around 2930 cm⁻¹ and 2852 cm⁻¹ which are attributed to adsorbed cyclohexane, while for the Al₂O₃ support, these peaks disappeared after 15 min of N₂ purging. Also, commercial CeO₂

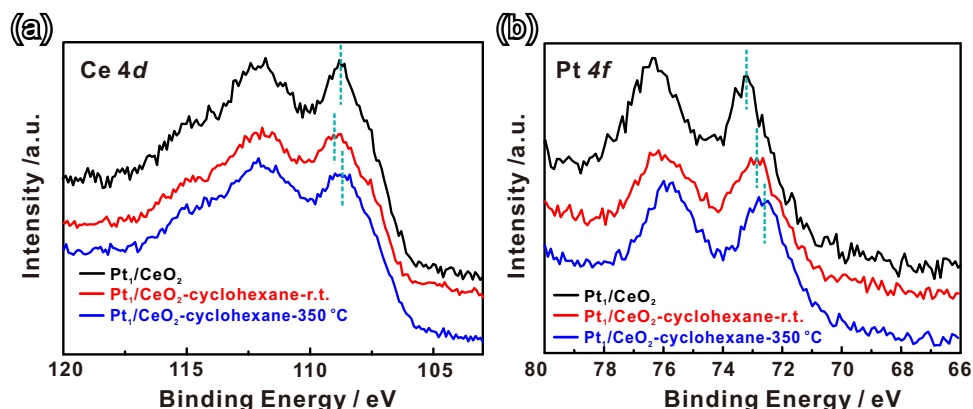


Fig. 4 In situ AP-XPS of Pt₁/CeO₂ catalyst. **a** Ce 4d and **(b)** Pt 4f APXPS spectra of Pt₁/CeO₂ catalysts in different conditions. The black, red, and blue lines are Pt₁/CeO₂ in vacuum, in 0.1 Torr cyclohexane at room temperature and 0.1 Torr cyclohexane at reaction temperature of 350 °C, respectively.

powders (Supplementary Fig. 10) were studied for cyclohexane adsorption using FTIR. We found that cyclohexane adsorption is very weak and all the cyclohexane desorbed during 10 min pure N₂ purging. To confirm the cyclohexane adsorption site on CeO₂, XPS was used to determine the Ce oxidation state in commercial CeO₂ powders compared to that in the as-prepared CeO₂ (Supplementary Fig. 11)⁴². The Ce 3d XPS spectra are very sensitive to its oxidation state, showing 10 peaks which are attributed to Ce³⁺ (881.0, 883.4, 899.3 and 903.1 eV) and Ce⁴⁺ (882.2, 888.4, 898.1, 900.7, 907.3 and 916.7 eV), which were used to calculate the concentration of Ce³⁺ in CeO₂^{32,43}. The results show that the O vacancies (V_O) in our CeO₂ nanorods is higher than that in the commercial powders. To further verify that V_O promote cyclohexane adsorption, we loaded Pt on commercial CeO₂ by the same ascorbic acid (AA) assisted reduction method, which created some V_O sites on CeO₂ at the same time (Supplementary Table 2). The Pt L₃-edge EXAFS showed that similar to the Pt₁/CeO₂ catalyst, Pt on the commercial CeO₂ particles was also a single site (Supplementary Fig. 5). The in situ DRIFTS (Supplementary Fig. 9) showed that the higher V_O concentration improved the cyclohexane adsorption ability, causing the Pt₁/CeO₂-commercial catalyst activity to be comparable to the activity of Pt₁/CeO₂ catalyst at lower temperature (200 °C).

Ambient-pressure X-ray photoelectron spectroscopy (AP-XPS).

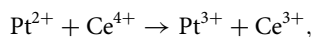
To identify the nature of the active site in Pt₁/CeO₂ during reaction, AP-XPS was employed to measure the valence state change of Pt and Ce during cyclohexane dehydrogenation. Fig 4a shows the Ce 4d spectra of Pt₁/CeO₂ catalysts under different conditions⁴⁴. We expect the lowest binding energy peak for Ce⁴⁺ at 109.3 eV and for Ce³⁺ the stronger peak in this range appears at 108.0 eV (with a much weaker peak at 105.4 eV)⁴⁵. Based on the measured line shape, we can see a slightly increasing Ce³⁺ population with cyclohexane dosing and increased temperature, which was also confirmed by the NEXAFS results at the Ce M_{4,5} edge after absorbing cyclohexane (Supplementary Fig. 12). Knowing from our FTIR results (Supplementary Fig. 9) that cyclohexane adsorption is driven by oxygen vacancies in our catalyst, after dosing 0.1 Torr of cyclohexane vapor, the binding energy of Ce⁴⁺ 4d shifted to slightly higher energy, which we ascribe to surface polarization of CeO₂ due to adsorbates (Fig. 4a). With further increase of the temperature to 350 °C, which causes hydrogen generation from cyclohexane dehydrogenation, and driving off adsorbates, we notice that the Ce⁴⁺ 4d peak shifts back to a lower energy⁴⁶. The Pt 4f XPS reveals lower binding energy peaks ranging from 73.2 to 72.9 to 72.6 eV, slightly above

measured PtO peaks at 72.2 eV (PtO₂ appears at 74.5 eV)⁴⁷. One possibility is that we may be seeing Pt³⁺ (reported 4f binding energy of Pt³⁺ is 73.3 eV)⁴⁸ due to chemical bonds formed with Pt²⁺ active sites (possibly remaining ligands on the as-prepared sample)—see our mechanism below. By contrast with Pt L₃ XANES, lower binding energy 4f XPS is extremely surface sensitive and highlights a lower oxidation state dominance at the surface. After introducing 0.1 Torr cyclohexane, and then increasing the temperature, we see a slight reduction in Pt 4f binding energy, which is evident as a slight reduction in valence charge due to the presence of adsorbates in our density functional theory (DFT) calculations. We saw no evidence for metallic Pt in any of these spectra (peak at 70.8 eV) which speaks to the stability of our catalyst at high operating temperatures.

Mechanism. The incorporation of the Pt atom into the ceria surface, by replacing a surface Ce atom, moves well beyond the strong metal-support interactions that might be expected for supported metal nanoparticles or clusters. Therefore, the traditional metal-support interaction and reaction models which were built based on the surface/interface of metal nanoparticles and support, can no longer precisely describe the interactions and reaction occurring in the local environment of a single metal atom^{49,50}. Our results, combining the characterization data reported above and DFT calculations of model catalyst reactions, show that the combination of (1) the incorporated Pt site, (2) a neighboring oxygen vacancy, and (3) the variable redox of Ce provide the necessary flexibility to catalyze multiple reactions. Specifically, the combination of these three components in the single-site Pt₁/CeO₂ catalyst enables: adsorption, activation, and reaction of reactant (cyclohexane); H species spillover; and H₂ reformation. We refer to this as a super-synergistic effect, by contrast with synergistic catalysis⁵¹, in which two distinct catalysts can enhance reactions between two different reactants.

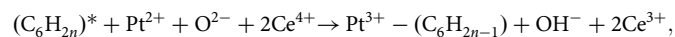
The in situ FTIR and AP-XPS results indicate that the ceria support, especially the abundance of oxygen vacancies, plays a significant role during cyclohexane adsorption and dehydrogenation. In a perfect crystal of CeO₂, the formal oxidation state of Ce is Ce⁴⁺ with no oxygen vacancies and Pt substitution for Ce would nominally place it in the same Pt⁴⁺ oxidation state, but, in combination with an oxygen vacancy^{52,53}, our DFT calculations show that the Pt 5d unoccupied orbitals lie just lower in energy than the Ce 4f orbitals, and so the two excess valence electrons released by the O vacancy reduce Pt⁴⁺ to Pt²⁺, which adopts the signature of the planar PtO₄ coordination of Pt²⁺ by breaking bonds with two ceria O atoms (Supplementary Fig. 20). We propose that the super-synergistic coupling between the

single-atom Pt and the ceria support with oxygen vacancy is driven by redox coupling (or disproportionation) between both the metal ions:



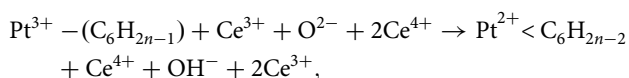
which is vital for forming chemical bonds between formally radical intermediates and the single-site Pt. We propose two dominant reactions for cyclohexane dehydrogenation:

(1) Hydrogen abstraction and Pt–C bond (denoted as Pt–C bond) formation:



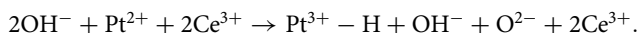
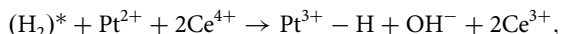
where $n = 6, 5, 4$. Removal of a neutral H atom from the organic group would nominally produce two radicals. The (neutral) H atom sheds its electron to form Ce^{3+} and joins the oxide dianion to produce a hydroxide ion (OH^-) (Supplementary Figs. 15, 16). The $5d^8$ electronic configuration of Pt^{2+} cannot bind with the organic radical, so it sheds an electron to form another Ce^{3+} and accepts the radical's electron into a now half-filled $5d$ orbital, forming a strong bond with the C atom of the adsorbate.

(2) H abstraction and Pt < C = C bond (denoted as Pt < C=C bond) formation:



where $n = 6, 5, 4$ again. In this case, the Pt reverts to its original Pt^{2+} oxidation state and bonds with the π electrons of a C=C double bond, effectively bonding with both the carbon atoms. In the process, the Pt atoms rotates its bonding plane to meet the C=C double bond by breaking two O bonds and forming one new O bond (Supplementary Fig. 17). The high cation coordination of the cubic ceria crystal provides this flexibility for the Pt to adjust its bonding environment and make these two very different bonds to accommodate saturated and unsaturated hydrocarbons both present in dehydrogenation products.

We also propose an analogous super-synergy exists for the dehydrogenation of the catalyst surface, to dissociate H_2 or recombine protons and electrons into H_2 molecules via a Pt–H bound intermediate (Supplementary Fig. 18):



To summarize this analysis derived from DFT calculations, the super-synergy results from: the incorporation of a Pt atom by substitution at a surface Ce site; a neighboring oxygen vacancy; and the variable redox of Ce. The major features of super-synergy are as follows: (1) The exchange of electrons between the active Pt site and the ceria support permits facile switching of the function of the Pt atom in binding directly to a single C atom of a radical adsorbate versus binding to a pair of atoms in a C=C double bond of a non-radical adsorbate; (2) The disproportionation between Pt and Ce oxidation states facilitates H abstraction or addition via spillover (with similar duality for dissociation or recombination of H_2); and (3) the reducible ceria support acts as a reservoir for abstracted hydrogen to permit serial dehydrogenation of adsorbed aromatics followed by reformation and release of H_2 .

Now, we can sequentially combine these reactions (Fig. 5) to reveal how Pt_1/CeO_2 favorably dehydrogenates cyclohexane to produce benzene, without the need for multiple catalytic sites due to the super-synergy just described. Both cyclohexane and benzene exhibit reasonable physisorption energies (-18.8 and -15.9 kcal/mol, respectively, from DFT calculations) due to the presence of oxygen vacancies and validated above using DRIFTS and X-ray spectroscopy. This is welcome, as our previous study

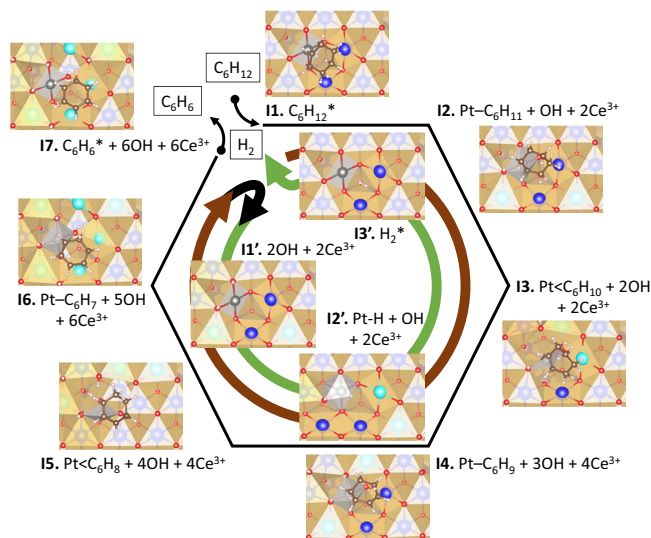


Fig. 5 Cyclohexane dehydrogenation pathway on Pt_1/CeO_2 catalyst.

Proposed cyclohexane dehydrogenation pathway (brown arrow) on Pt_1/CeO_2 at an O vacancy (V_O) involving H abstraction to the catalyst surface (as OH^-) with associated formation of small polarons (Ce^{3+}) followed by recombination and release of H_2 (green arrow). Reaction intermediates are labeled as **11–17** (dehydrogenation) and **11'–13'** (H_2 release), with relative energies provided in Supplementary Fig. 19 of the Supporting Information. Structural snapshots are provided for each intermediate. Ce^{4+} : light blue (sub-surface) and dark blue (surface); Ce^{3+} : turquoise; Pt: gray; O: red; H: white.

showed that single metal sites had poor adsorption of molecules such as CO^{26} . However, the mechanism here is clearly dominated by the successive exothermic formation of strongly bound surface hydroxy anions (Supplementary Fig. 19). In principle, in the absence of kinetic data (i.e., activation energies), the thermodynamic driving force is present to advance the dehydrogenation. Usually, H_2 reformation from a metal oxide surface is the rate-determining step for hydrocarbon dehydrogenation and requires high reaction temperatures^{54,55}, fortunately, due to the presence of the single-atom Pt site, the energy cost for H_2 reformation and desorption is reduced significantly (Supplementary Fig. 19). At functional temperatures, the saturated local environment around each Pt single-site can be purged by releasing H_2 gas and the next cyclohexane molecule can be processed. Similarly, for hydrogenation of benzene, the favorable dissociation of physisorbed H_2 will enrich the vicinity of the Pt single-site with available hydrogen that can then begin to resaturate benzene. Now it is the uphill process of cyclohexane reformation that requires high temperatures.

As shown in Supplementary Fig. 9, the commercial CeO_2 , which has a low oxygen vacancy concentration, has very poor capacity for cyclohexane adsorption. With the ascorbic acid treatment, Pt single sites are formed together with O vacancies in the support, which promotes the adsorption of cyclohexane. The calculated adsorption energies of cyclohexane on CeO_2 slab, CeO_2 slab with one oxygen vacancy, Pt_1/CeO_2 slab and Pt_1/CeO_2 slab with one oxygen vacancy are -10.5 , -14.8 , -11.8 , -18.8 kcal/mol, respectively. However, the super-synergy between Pt and Ce cations is also vital. This explains why on the inert support of Al_2O_3 , there is no cyclohexane adsorption (no vacancies), and dehydrogenation of cyclohexane at low temperature does not occur (Al^{3+} cannot easily change oxidation state). In contrast, the Pt nanoparticles on Al_2O_3 show detectable dehydrogenation reaction of cyclohexane, due to typical metal surface catalysis⁴⁸. These results clearly outline stark differences between the dehydrogenation mechanisms of single Pt

sites and Pt nanoparticles. At last, compared with cyclohexane, intermediates such as cyclohexene and cyclohexadiene have been reported to be more active and easier to dehydrogenate to benzene^{52,53}. Indeed, our calculated energetics (Supplementary Fig. 19) indicate that these intermediate cyclic alkenes (**I3** and **I5** in Fig. 5) are increasingly stable on the path towards generating the triene, benzene. The only uphill process is the generation of the penultimate intermediate, C₆H₇. However, given that all species are strongly bound to the surface, this helps explain the observed high selectivity (100%) towards benzene, at high temperature (Fig. 2b).

Benzene hydrogenation. An ideal LOHC system would feature both the hydrogen-rich and hydrogen-deficient organic compounds as liquids. And the usage of a proper catalytic system would allow for the efficient release of hydrogen by promoting the dehydrogenation reaction, and recovery of the hydrogen depleted by dehydrogenation. Hence, hydrogenation of benzene by the same single Pt₁/CeO₂ catalyst was investigated. As shown in the literature, high temperature and low pressure favor the dehydrogenation, and, reversibly, high H₂ pressure and relatively low temperature favor the rehydrogenation. Therefore, in our study, which is different from these dehydrogenation reactions, dehydrogenation was carried out in gas-phase fixed-bed reactor with ambient pressure at a temperature of 350 °C, the hydrogenation reactions were carried out in a liquid-phase batch reactor with a low reaction temperature (60–120 °C) and high H₂ pressure (3.40–27.22 atm). Interestingly, for the benzene hydrogenation reaction, the single-site Pt₁/CeO₂ catalyst showed excellent catalytic activity, much higher than that of Pt nanoparticle catalysts (2.5 nm Pt/CeO₂ and 7 nm Pt/CeO₂) (Fig. 6)⁵⁶. We further tested Pt₁/CeO₂ catalytic properties under different reaction conditions (Supplementary Fig. 13). Under 27.22 atm H₂ and at 120 °C, with a molar ratio of H₂ to benzene of 5 to 1 in the batch reactor, we found that 50% of the benzene could be rehydrogenated. Our experiments indicate that conversion of benzene increases with reaction temperature and hydrogen pressure, as well as with the ratio of H₂ to benzene. Therefore, a higher conversion (>99%) of rehydrogenation of benzene or toluene could be anticipated by further optimizing the reaction conditions (especially with high H₂ pressure).

Reversible dehydrogenation/hydrogenation of methylcyclohexane/toluene. In the practical application of liquid cyclohexane as carrier to store and transport hydrogen, the dehydrogenation product, benzene, is classified as a carcinogen. By comparison,

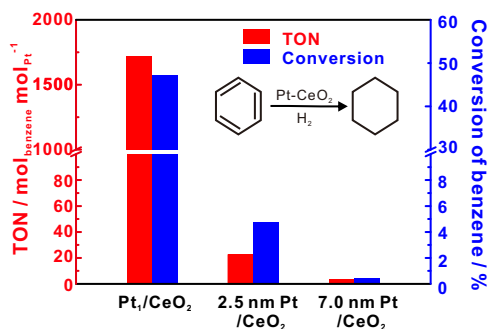


Fig. 6 Catalytic benzene hydrogenation performance of on Pt₁/CeO₂ and related catalyst. Catalytic benzene hydrogenation on Pt–CeO₂ catalysts (Pt₁/CeO₂, 2.5 nm Pt/CeO₂, and 7 nm Pt/CeO₂). Turnover number (TON) of benzene conversion per Pt site for 8 h and conversion of benzene on different Pt–CeO₂ catalysts. Reaction conditions: 40 mg catalysts dispersed in 3 mL *n*-heptane; addition of 100 μL of benzene in 27.22 atm of hydrogen gas at 120 °C and stirred for 8 h.

toluene, the dehydrogenation product of methylcyclohexane, although with a similar structure as benzene, has much lower toxicity. Strikingly, we found that, during the methylcyclohexane dehydrogenation, the Pt₁/CeO₂ single-site catalyst also exhibited outstanding catalytic activity for dehydrogenation. Under the reaction conditions (350 °C), the TOF of hydrogen production was about 29,300 mol_{H₂} mol_{Pt}⁻¹ h⁻¹ without any other by-products. As for toluene hydrogenation, 800 mol_{toluene} mol_{Pt}⁻¹ was achieved under relatively mild reaction conditions (Fig. 7 and Supplementary Fig. 14). That means this efficient single-site Pt₁/CeO₂ catalyst can be also applied in methylcyclohexane/toluene reversible hydrogen storage and transportation^{57,58}.

In summary, we demonstrated the advantages of ensemble reaction sites formed by a single Pt atom and surrounding oxygen vacancies, Pt₁/CeO₂, for the dehydrogenation and rehydrogenation of large molecule reactants such as cyclohexane and methylcyclohexane. Compared to nanoparticles catalysts (2.5 nm and 7.0 nm size Pt particles on CeO₂ and commercial 5% Pt/Al₂O₃), the Pt₁/CeO₂ catalyst exhibits greatly enhanced reaction rates of cyclohexane dehydrogenation, 309 times higher than that of conventional supported Pt nanoparticles. At the same time, the single-site Pt₁/CeO₂ catalyst also has significantly higher activity in the reaction of benzene hydrogenation. Moreover, this single-site catalyst was highly efficient in the dehydrogenation and hydrogenation of other aromatics, such as methylcyclohexane/toluene system for hydrogen generation and storage.

The combined results of in situ DRIFTS, APXPS, and EXAFS presented here demonstrate that the electronic properties and catalytic activity of our single-site Pt₁/CeO₂ catalyst can be precisely assigned to specific interactions between Pt atoms and neighboring surface atoms of the substrate. The mechanism predicted by our DFT studies is described as super synergistic. Unlike Pt nanoparticle catalysts, our single-site Pt₁/CeO₂ catalyst facilitates strong adsorption of large reactants due to surface oxygen vacancies that provide direct access to binding to the Pt site. Redox coupling between Pt and Ce ions and switchable O coordination environments permit alternating binding to radical and unsaturated by-products of H abstraction/addition. Spillover of H atoms to the CeO₂ (111) surface is reversible via the Pt site and the same redox switching mechanism. And so, this combination can facilitate multiple reactions at a single site. Our results expand the application range of single-site catalyst to include large molecular reactants. They also highlight the versatility of a single-site catalyst for driving multiple reactions, paving the way for further rational design of highly efficient catalysts for sustainable energy generation and storage.

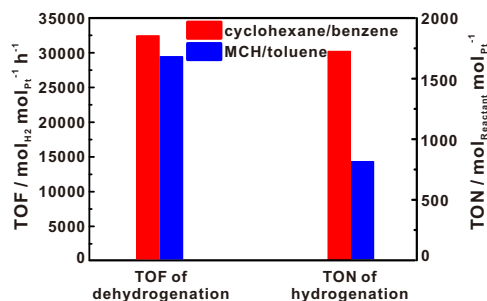


Fig. 7 Comparisons of dehydrogenation and hydrogenation efficiency of different molecules. Dehydrogenation reaction conditions: 100 mg catalyst mixed with 500 mg sand; Gas flow: N₂ 30 ml/min; Methylcyclohexane feeding rate: 3 mL/h; temperature: 350 °C. Hydrogenation reaction conditions: 40 mg catalyst dispersed in 3 mL *n*-heptane; added 100 μL toluene under 27.22 atm hydrogen at 120 °C and stirred for 12 h.

Methods

Catalyst preparation. The isolated single Pt sites on CeO₂ (Pt₁/CeO₂) were fabricated by a modified ascorbic acid (AA)-assisted reduction method. The porous CeO₂ nanorods were first synthesized according to previous reports. 500 mg as-prepared CeO₂ was dispersed in 175 mL distilled water, 1 mmol (0.176 g) AA was added, and the solution was stirred at room temperature for 3 h. The collected products were washed with distilled water several times and dried in vacuum, denoted as CeO₂-AA. Second, 140 mg CeO₂-AA powder was dispersed in 55 mL distilled water and 0.4 mL (10 mg/mL) H₂PtCl₆ solution was added to it. After stirring for 3 h at room temperature, the products were collected and washed with water. After drying in vacuum, the products were calcined at 300 °C for 1 h in air to remove excess AA.

Dehydrogenation of cyclohexane. The catalytic activity of catalysts toward hydrogen production from cyclohexane was performed in a continuous flow reactor. In a typical catalytic measurement, the 100 mg catalyst was placed in a U-shape fixed-bed flow reactor after mixing with 500 mg white quartz (50–70 mesh particle size). The feed of 30 mL/min N₂ regulated by a mass flow controller to be at 1 atm and feed of 3 mL/h cyclohexane controlled by an injection pump were mixed together and directed towards the catalysts. The temperature of bed was monitored by a K-type thermocouple controlled by a PID 679 controller. The products were analyzed online by HP 5890 GC (hayesep D column and hayesep Q column) equipped with TCD and FID detector. Besides, the liquid products were also collected and measured by NMR (AV-700).

The turnover frequency (TOF) is calculated using the following equation:

$$\text{TOF} = \frac{\text{Hydrogen Production}}{\text{Number of active Pt Sites} \times \text{time}} \quad (1)$$

Hydrogenation of benzene. The catalytic activity of benzene hydrogenation was performed in BioTage Endeavor parallel pressure reactor. In a typical catalytic measurement, 40 mg catalyst was dispersed in 3 mL *n*-heptane, then 100 μL benzene was added to the solution. After stirring the reaction mixture at 120 °C for 8 h under 27.22 atm hydrogen, the product was analyzed by NMR (AV-700).

The conversion and turnover number (TON) are calculated using the following equations:

$$\text{Conversion} = \frac{\text{Output of Cyclohexane}}{\text{Input of Benzene}} \times 100\% \quad (2)$$

$$\text{TON} = \frac{\text{Cyclohexane Production}}{\text{Number of active Pt Sites} \times \text{time}} \quad (3)$$

Received: 6 December 2021; Accepted: 20 January 2022;

Published online: 01 March 2022

References

- Munnik, P. et al. Recent developments in the synthesis of supported catalysts. *Chem. Rev.* **115**, 6687–6718 (2015).
- Tauster, S. J. Strong metal-support interactions. *Acc. Chem. Res.* **20**, 389–394 (1987).
- Xie, C. et al. Surface and interface control in nanoparticle catalysis. *Chem. Rev.* **120**, 1184–1249 (2019).
- Conner, W. C. Jr. et al. Spillover in heterogeneous catalysis. *Chem. Rev.* **95**, 759–788 (1995).
- Nie, L. et al. Activation of surface lattice oxygen in single-atom Pt/CeO₂ for low-temperature CO oxidation. *Science* **358**, 1419–1423 (2017).
- Nielsen, M. et al. Low-temperature aqueous-phase methanol dehydrogenation to hydrogen and carbon dioxide. *Nature* **495**, 85–89 (2013).
- Yao, S. et al. Atomic-layered Au clusters on α-MoC as catalysts for the low-temperature water-gas shift reaction. *Science* **357**, 389–393 (2017).
- Qiao, B. et al. Single-atom catalysis of CO oxidation using Pt₁/FeO_x. *Nat. Chem.* **3**, 634–641 (2011).
- Yang, X. F. et al. Single-atom catalysts: a new frontier in heterogeneous catalysis. *Acc. Chem. Res.* **46**, 1740–1748 (2013).
- Chen, Y. et al. Single-atom catalysts: synthetic strategies and electrochemical applications. *Joule* **2**, 1242–1264 (2018).
- Wang, A. et al. Heterogeneous single-atom catalysis. *Nat. Rev. Chem.* **2**, 65–81 (2018).
- Jones, J. et al. Thermally stable single-atom platinum-on-ceria catalysts via atom trapping. *Science* **353**, 150–154 (2016).
- Shan, J. et al. Mild oxidation of methane to methanol or acetic acid on supported isolated rhodium catalysts. *Nature* **551**, 605–608 (2017).
- Liu, P. et al. Photochemical route for synthesizing atomically dispersed palladium catalysts. *Science* **352**, 797–800 (2016).
- Jeong, H. et al. Highly durable metal ensemble catalysts with full dispersion for automotive applications beyond single-atom catalysts. *Nat. Catal.* **3**, 368–375 (2020).
- Jeong, H. et al. Fully dispersed Rh ensemble catalyst to enhance low-temperature activity. *J. Am. Chem. Soc.* **140**, 9558–9565 (2018).
- Yu, K. et al. Asymmetric oxygen vacancies: the intrinsic redox active sites in metal oxide catalysts. *Adv. Sci.* **7**, 1901970 (2020).
- Li, T. et al. Maximizing the number of interfacial sites in single-atom catalysts for the highly selective, solvent-free oxidation of primary alcohols. *Angew. Chem. Int. Ed.* **57**, 7795–7799 (2018).
- Wang, L. et al. Single-site catalyst promoters accelerate metal-catalyzed nitroarene hydrogenation. *Nat. Comm.* **9**, 1–8 (2018).
- Steele, B. C. H. et al. Materials for fuel-cell technologies. *Nature* **414**, 345 (2001).
- Tromp, T. K. et al. Potential environmental impact of a hydrogen economy on the stratosphere. *Science* **300**, 1740–1742 (2003).
- Schultz, M. G. et al. Air pollution and climate-forcing impacts of a global hydrogen economy. *Science* **302**, 624–627 (2003).
- Tseng, P. et al. A hydrogen economy: opportunities and challenges. *Energy* **30**, 2703–2720 (2005).
- Teichmann, D. et al. A future energy supply based on Liquid Organic Hydrogen Carriers (LOHC). *Energy Environ. Sci.* **4**, 2767–2773 (2011).
- Markiewicz, M. et al. Environmental and health impact assessment of Liquid Organic Hydrogen Carrier (LOHC) systems—challenges and preliminary results. *Energy Environ. Sci.* **8**, 1035–1045 (2015).
- Chen, L. N. et al. Efficient hydrogen production from methanol using a single-site Pt₁/CeO₂ catalyst. *J. Am. Chem. Soc.* **141**, 17995–17999 (2019).
- Preuster, P. et al. Liquid organic hydrogen carriers (LOHCs): toward a hydrogen-free hydrogen economy. *Acc. Chem. Res.* **50**, 74–85 (2017).
- Modisha, P. M. et al. The prospect of hydrogen storage using liquid organic hydrogen carriers. *Energy Fuels* **33**, 2778–2796 (2019).
- Solowey, D. P. et al. A new and selective cycle for dehydrogenation of linear and cyclic alkanes under mild conditions using a base metal. *Nat. Chem.* **9**, 1126–1132 (2017).
- Nakaya, Y. et al. Active, selective, and durable catalyst for alkane dehydrogenation based on a well-designed trimetallic alloy. *ACS Catal.* **10**, 5163–5172 (2020).
- Okada, Y. et al. Development of dehydrogenation catalyst for hydrogen generation in organic chemical hydride method. *Int. J. Hydrog. Energy* **31**, 1348–1356 (2006).
- Chen, J. et al. Surface engineering protocol to obtain an atomically dispersed Pt/CeO₂ catalyst with high activity and stability for CO oxidation. *ACS Sustain. Chem. Eng.* **6**, 14054–14062 (2018).
- Ravel, B. et al. ATHENA, ARTEMIS, HEPHAESTUS: data analysis for X-ray adsorption spectroscopy using IFEFFIT. *J. Synchrotron Radiat.* **12**, 537–541 (2005).
- Sethapum, W. et al. Genesis and evolution of surface species during Pt atomic layer deposition on oxide supports characterized by in situ XAFS analysis and water–gas shift reaction. *J. Phys. Chem. C* **114**, 9758–9771 (2010).
- Schildhauer, T. et al. The equilibrium constant for the methylcyclohexane–toluene system. *J. Catal.* **198**, 355–358 (2001).
- Liu, J. C. et al. Theoretical understanding of the stability of single-atom catalysts. *Nat. Sci. Rev.* **5**, 638–641 (2018).
- Resasco, J. et al. Uniformity is key in defining structure–function relationships for atomically dispersed metal catalysts: the case of Pt/CeO₂. *J. Am. Chem. Soc.* **142**, 169–184 (2019).
- Jiang, Z. et al. Stabilizing platinum atoms on CeO₂ oxygen vacancies by metal-support interaction induced interface distortion: mechanism and application. *Appl. Catal. B* **278**, 119304 (2020).
- Kariya, N. et al. Efficient hydrogen production using cyclohexane and decalin by pulse-spray mode reactor with Pt catalysts. *Appl. Catal. A* **247**, 247–259 (2003).
- Zhang, Z. et al. Thermally stable single atom Pt/m-Al₂O₃ for selective hydrogenation and CO oxidation. *Nat. Commun.* **8**, 1–10 (2017).
- Chesters, M. A. et al. The infrared spectrum of cyclohexane adsorbed on Pt (111). *Spectrochim. Acta A* **46**, 1011–1016 (1990).
- Holgado, J. P. et al. Study of CeO₂ XPS spectra by factor analysis: reduction of CeO₂. *Appl. Surf. Sci.* **161**, 301–315 (2000).
- Bèche, E. et al. Ce 3d XPS investigation of cerium oxides and mixed cerium oxide (Ce_xTi_yO_z). *Surf. Interface Anal.* **40**, 264–267 (2008).
- Maslakov, K. I. et al. XPS study of ion irradiated and unirradiated CeO₂ bulk and thin film samples. *Appl. Surf. Sci.* **448**, 154–162 (2018).
- Mullins, D. R. et al. Electron spectroscopy of single crystal and polycrystalline cerium oxide surfaces. *Surf. Sci.* **409**, 307–319 (1998).
- Kato, S. et al. Quantitative depth profiling of Ce³⁺ in Pt/CeO₂ by in situ high-energy XPS in a hydrogen atmosphere. *Phys. Chem. Chem. Phys.* **17**, 5078–5083 (2015).

47. Han, K. N. et al. Development of Pt/TiO₂ nanohybrids-modified SWCNT electrode for sensitive hydrogen peroxide detection. *Sensors Actuators B: Chem.* **174**, 406–413 (2012).
48. Osaki, J. et al. Selective loading of platinum or silver cocatalyst onto a hydrogen-evolution photocatalyst in a silver-mediated all solid-state Z-scheme system for enhanced overall water splitting. *RSC Adv.* **9**, 41913–41917 (2019).
49. Qi, K. et al. Single atom is not alone: metal–support interactions in single-atom catalysis. *Mater. Today* **40**, 173–192 (2020).
50. van Deelen, T. W. et al. Control of metal–support interactions in heterogeneous catalysts to enhance activity and selectivity. *Nat. Catal.* **2**, 955–970 (2019).
51. Allen, A. E. et al. Synergistic catalysis: a powerful synthetic strategy for new reaction development. *Chem. Sci.* **3**, 633–658 (2012).
52. Blakely, D. W. et al. The dehydrogenation and hydrogenolysis of cyclohexane and cyclohexene on stepped (high miller index) platinum surfaces. *J. Catal.* **42**, 181–196 (1976).
53. Coperet, C. et al. Silica-supported, narrowly distributed, subnanometric PtZn particles from single sites with high propane-dehydrogenation performance. *Chem. Sci.* **11**, 1549–1555 (2020).
54. Dai, Y. et al. Recent progress in heterogeneous metal and metal oxide catalysts for direct dehydrogenation of ethane and propane. *Chem. Soc. Rev.* **50**, 5590–5630 (2021).
55. Liu, J. et al. Highly-dispersed zinc species on zeolites for the continuous and selective dehydrogenation of ethane with CO₂ as a Soft Oxidant. *ACS Catal.* **11**, 2819–2830 (2021).
56. Bratlie, K. M. et al. Platinum nanoparticle shape effects on benzene hydrogenation selectivity. *Nano Lett.* **7**, 3097–3101 (2007).
57. Wang, Y. et al. Pure hydrogen production by partial dehydrogenation of cyclohexane and methylcyclohexane over nanotube-supported Pt and Pd catalysts. *Energy Fuels* **18**, 1429–1433 (2004).
58. Boufaden, N. et al. Dehydrogenation of methylcyclohexane to toluene over partially reduced silica-supported Pt–Mo catalysts. *J. Mol. Catal. A: Chem.* **420**, 96–106 (2016).

Acknowledgements

This work was supported by the Hydrogen Materials Advanced Research Consortium (HyMARC), established as part of the Energy Materials Network by the U.S. Department of Energy (DOE), Office of Energy Efficiency and Renewable Energy, Fuel Cell Technologies Office, under Contract Number DE-AC02-05CH11231. This research used resources of the Advanced Light Source, which is a DOE Office of Science User Facility under the same contract. Work by L.C., P.V., Y.L., J.G. D.P., and J.S., was performed as part of a User Project at The Molecular Foundry of the Lawrence Berkeley National Laboratory, which is supported by the Office of Science of the U.S. Department of Energy also under the same contract. The Sandia National Laboratory is a multi-mission laboratory managed and operated by National Technology and Engineering Solutions of Sandia, LLC, a wholly owned subsidiary of Honeywell International, Inc., for the U.S. Department of Energy's National Nuclear Security Administration under Contract No. DE-NA-0003525. We thank Jeng-Lung Chen and Chih-Wen Pao in National Synchrotron Radiation Research Center (NSRRC) for the measurement and analysis of Pt

XANES spectra. For computational resources, we thank National Energy Research Scientific Computing Center (NERSC) and High-Performance Computing Services (HPCS) at Lawrence Berkeley National Laboratory.

Author contributions

L.C. performed the catalyst preparation and catalyst testing under the supervision of J.S. and G.A.S. K.H. and L.C. carried out the catalytic hydrogenation testing and NMR measurement of catalytic products. Z.Q. performed in situ FTIR and APXPS measurements. S.Z. carried out the TEM, XRD, and XPS measurements. Y.-S.L. and J.G. performed the XANES measurement and data analysis. D.P. and P.V. performed the calculations for the mechanism of cyclohexane dehydrogenation. L.C., V.S., M.D.A., L.Z. M.S., and J.S. conceived the idea. D.P., A.G.S., and J.S. supervised the project. All authors contributed to the data analysis and drafting of this manuscript.

Competing interests

The authors declare no competing interests.

Additional information

Supplementary information The online version contains supplementary material available at <https://doi.org/10.1038/s41467-022-28607-y>.

Correspondence and requests for materials should be addressed to David Prendergast, Gabor A. Somorjai or Ji Su.

Peer review information *Nature Communications* thanks the anonymous reviewer(s) for their contribution to the peer review of this work.

Reprints and permission information is available at <http://www.nature.com/reprints>

Publisher's note Springer Nature remains neutral with regard to jurisdictional claims in published maps and institutional affiliations.



Open Access This article is licensed under a Creative Commons Attribution 4.0 International License, which permits use, sharing, adaptation, distribution and reproduction in any medium or format, as long as you give appropriate credit to the original author(s) and the source, provide a link to the Creative Commons license, and indicate if changes were made. The images or other third party material in this article are included in the article's Creative Commons license, unless indicated otherwise in a credit line to the material. If material is not included in the article's Creative Commons license and your intended use is not permitted by statutory regulation or exceeds the permitted use, you will need to obtain permission directly from the copyright holder. To view a copy of this license, visit <http://creativecommons.org/licenses/by/4.0/>.

© The Author(s) 2022